Topological phase transitions of Thouless charge pumping realized in helical organic molecules with long-range hopping

Ai-Min Guo [1,*], Pei-Jia Hu [1], Xiao-Hui Gao,[1] Tie-Feng Fang [2,†] and Qing-Feng Sun[3,4,5]

[1]*Hunan Key Laboratory for Super-microstructure and Ultrafast Process, School of Physics and Electronics, Central South University, Changsha 410083, China*

[2]*Key Laboratory for Magnetism and Magnetic Materials of MOE, School of Physical Science and Technology, Lanzhou University, Lanzhou 730000, China*

[3]*International Center for Quantum Materials, School of Physics, Peking University, Beijing 100871, China*

[4]*Collaborative Innovation Center of Quantum Matter, Beijing 100871, China*

[5]*CAS Center for Excellence in Topological Quantum Computation, University of Chinese Academy of Sciences, Beijing 100190, China*

Recent studies indicated that helical organic molecules, such as DNA and the α-helical protein, can behave as Thouless quantum pumps when a rotating electric field is applied perpendicularly to their helical axes. Here we investigate the influence of long-range hoppings on this topological pumping of electrons in single-helical organic molecules. Under variation of the long-range hoppings governed by a decay exponent μ, we find an energy gap in the molecular band structure closes at a critical value μ_c of the decay exponent and reopens for μ deviating from μ_c. The relevant bulk bands in a pumping cycle acquire different Chern numbers in the strong ($\mu < \mu_c$) and weak ($\mu > \mu_c$) long-range hopping regimes, with a sudden jump at criticality. This topological phase transition is also shown to separate two distinct behaviors of the midgap end states in the pumping process. The end states carry quantized current pumped by the rotating electric field, and the current forms a plateau by sweeping the Fermi energy over the gap. In the strong-hopping phase, the quantized current plateau is positive, which is reversed to a negative one with smaller amplitude in the weak-hopping phase. However, the reversal is a smooth crossover, not a sharp transition, due to the finite sizes of the molecules. We show that these transport characteristics of the topological phase transition could also be observed at finite temperatures.

I. INTRODUCTION

Topology is a mathematical concept that describes some invariant properties of geometrical objects when they are smoothly deformed. The study of topological physics began with the discoveries of the integer [1] and fractional [2] quantum Hall effects and the gapped quantum spin-liquid state of integer-spin chains [3–5]. The integer quantum Hall effect defines a first topological phase that is distinct from all states of matter known before. In this effect, the quantized Hall conductance carried by chiral edge states is a topological invariant independent of material details [6,7]. When the time-reversal symmetry is preserved, some spin-orbit coupled systems can support exotic topological insulating states [8–14], which further enrich our understanding of topological phases of matter. Topological concepts can also be applied to unconventional superconductors [14], superfluids [15–17], and nodal systems [18–20]. Indeed, it has now become apparent that topological phenomena are essentially a ubiquitous property of physical systems in diverse fields, including condensed-matter physics, ultracold atomic gases [21], photonics [22], polaritonics [23], and even classical mechanics [24]. For gapped topological quantum materials, the global structure of the wave function, characterized by a topological invariant, remains unchanged

under variations of system parameters, unless the gap is closed at a topological phase transition. This wave function topology manifests itself as gapless states localized at the system boundary. Interestingly, topological invariants, such as the Chern number, can count the number of particles that are pumped through a spatially periodic system that is driven periodically and adiabatically in time. This topological quantum pumping, first introduced by Thouless in 1983 [25], was recently demonstrated in ultracold atomic experiments [26,27].

While most existing studies of topological phases of matter are based on inorganic materials, recent works [28,29] have proposed that topological states can also emerge in helical organic or bioorganic molecules. A distinct feature of these molecules, such as DNA and the α-helical protein, is their unique helical structures. Due to this helical symmetry, the α-helical protein and DNA provide direct realizations [28] of the topological Thouless pump driven by a rotating electric field applied perpendicularly to their helical axes. The pumped current through these molecules exhibits quantized plateaus by sweeping the Fermi energy over band gaps, which are topologically protected against perturbations [28]. It has further been shown that single-stranded DNA in the vicinity of a conventional superconductor can support topologically nontrivial superconducting phases hosting Majorana zero modes at the ends [29]. These fascinating results may stimulate more research interest in exploring topological physics of bioorganic systems. On the other hand, DNA- and protein-based structures have been extensively studied as promising candidates

---

*aimin.guo@csu.edu.cn

†fangtiefeng@lzu.edu.cn

for functional nanoelectronic devices [30–34]. In comparison with inorganic materials, such organic systems exhibit great flexibility. They can be easily bent, stretched, and twisted [35–39], allowing a mechanical modulation of the amplitude of electron hopping. It is now clear that in biological molecular systems, electronic transport via long-range hoppings, in addition to the nearest-neighbor one, can be significant [34], which has already played an important role in generating spin-selective phenomena in the protein and DNA [40–43]. This motivates us to address the influence of long-range electron hoppings on the topological phases of these helical molecules, and the long-range effect was, indeed, considered in the DNA topological superconductors [29]. Nevertheless, interesting questions remain about whether helical organic molecules with long-range hoppings can still implement a Thouless quantum pump and, if so, how its topological nature and current characteristics are modified.

The inclusion of long-range hoppings in systems without helical geometry has already been studied in the literature. It is shown that while second-neighbor hopping has a strong impact on the defect scattering in Schrödinger chains [44], one-dimensional metacrystals with long-range hoppings can support robust unidirectional transport [45]. In the layered honeycomb lattice Na_2IrO_3 [46] and a generalized Su-Schrieffer-Heeger chain [47], the change in long-range hoppings has been shown to drive a transition from trivial normal to nontrivial topological phases. Also topological adiabatic pumping itself has been addressed, mostly in the context of photonic waveguide arrays and optical lattices [22,26,27,48–50]. Particularly, Xu *et al.* [50] explored the pumping of atoms trapped in an optical lattice and predicted a topological phase transition when the second-neighbor hopping amplitude equals the first-neighbor one. Their scheme relied on simultaneously applying a high-frequency tilt oscillation and a slow temporal variation to the lattice and a somewhat tricky *in situ* detection of the center of mass of the atomic cloud. However, as elucidated in the following, our helical-molecule scheme resorts to only a single rotating electric field and allows the well-established transport measurement of relevant physical processes.

In this paper, we study the topological Thouless pump in helical organic molecules by explicitly taking into account the long-range electron hoppings. It is demonstrated that while the adiabatical charge pumping still occurs by the rotating electric field, the long-range hoppings, which decay exponentially, can induce a topological phase transition with transport features appearing in the pumped current through the lead-molecule-lead setup. The phase transition is characterized by the closure of a band gap at the critical decay exponent, separating two topologically nontrivial phases with strong and weak long-range hoppings. We show that the Chern invariants of the bulk bands adjacent to the gap and the evolution of midgap end states in the pumping process indicate clear differences between these two phases of the helical molecules. In particular, the strong- and weak-hopping phases support the transport of pumped electrons through the molecule in opposite directions, giving rise to two quantized current plateaus with different signs and amplitudes, as set by the sum over the Chern numbers of all the filled bands below the gap. However, a sharp reversal of the pumped current plateau
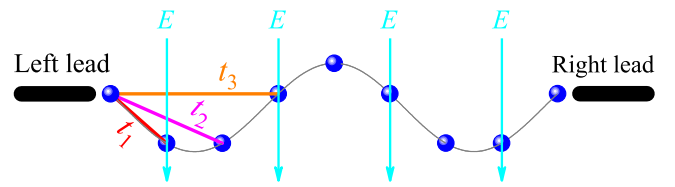

FIG. 1. Schematic representation of a single-helical molecule coupled with two external electrodes in the case of large helical pitch. The blue balls are local sites that can represent, e.g., amino acids for α-helical proteins and nucleobases for single-stranded DNA molecules. The intersite electron hoppings, t_1, t_2, t_3, . . . , are determined by Euclidean distances between sites. When a rotating electric field with uniform amplitude E is applied perpendicularly to the helical axis, the molecule can behave as a Thouless topological pump.

is absent near the topological phase boundary. It features instead a smooth crossover due to the finite-size effect. The experimental observability of these transport characteristics at finite temperatures is discussed.

The remainder of the paper is organized as follows. Section II introduces the model Hamiltonian for the Thouless pump realized in single-helical organic molecules with long-range hoppings and explains some necessary details of the computational scheme. Numerical results are presented in Sec. III. Section III A analyzes the bulk bands and end states of the system, revealing a topological phase transition induced by the long-range hoppings. We discuss consequences of the topological phase transition in the pumped current in Sec. III B. Finally, Sec. IV is devoted to a conclusion.

II. MODEL AND METHOD

The α-helical protein and singe-stranded DNA molecules possess similar helical structures. In the presence of the long-range hoppings and a rotating electric field perpendicular to their helical axes, as shown in Fig. 1, these single-helical organic molecules are modeled by the following Hamiltonian [28,40,51–53]:

$$\mathcal{H}(t) = \sum_{n=1}^{N} \varepsilon_n(t) c_n^\dagger c_n + \sum_{n=1}^{N-1} \sum_{j=1}^{N-n} t_j (c_n^\dagger c_{n+j} + c_{n+j}^\dagger c_n). \quad (1)$$

Here $c_n^\dagger$ (c_n) creates (annihilates) an electron with energy $\varepsilon_n(t)$ at site n, and the total number of sites, i.e., the molecular length, is denoted by N. The sites represent the amino acids for the protein and the nucleobases for the DNA. t_j is the hopping amplitude between the nth site and the $(n + j)$th site. A precise description of the long-range hopping strength requires taking into account the Euclidean distance between remote sites and the symmetry of local orbitals [29,40]. This would involve too many parameters. For the purpose of introducing a minimal model for helical molecules that already captures qualitatively new features, we restrict ourselves to the special case of large helical pitches, where the Euclidean distance of a site to its jth neighbor monotonically increases with j, as shown in Fig. 1. One can thus approximately take the long-range hopping amplitude, $t_j = t_1 e^{-\mu(j-1)}$, which exponentially decays with site index, as characterized by μ the decay exponent. Note that the previous helical-molecule

realization [28] of topological pumping took into account only the nearest-neighbor hopping t_1 (i.e., $\mu \to \infty$). Since in realistic protein, DNA, and other helical organic molecules the decay exponent μ is very different, we thus treat μ as a variable parameter in the model study. This is also inspired by the fact that in experiments μ can be tuned to a large degree by stretching and twisting the helical molecules and thus changing their intersite distances [35–39].

Effects of the helical structure and the rotating electric field are manifested in the time-dependent on-site energy $\varepsilon_n(t)$, which reads [54,55]

$$\varepsilon_n(t) = V_g \cos[n\phi_0 - \varphi(t)], \qquad (2)$$

where $V_g = eER$ describes the half energy difference across the molecules along the direction of the electric field E, R denotes the cross-sectional radius of the molecules, ϕ_0 is the twist angle between two neighboring sites in the cross section, and the phase $\varphi(t) = 2\pi f t$ represents the orientation of the electric field, with f being the rotational frequency. In the absence of long-range hoppings, i.e., $t_j = 0$ for $j > 1$, the Hamiltonian (1) is, equivalently, a dimension-reduced mapping of the Harper-Hofstadter model [56,57] describing a quantum Hall system in a two-dimensional square lattice. In this mapping, the twist angle $\phi_0/2\pi$ corresponds to the magnetic flux per primitive cell in units of the flux quantum, and the direction of the electric field $\varphi(t)$ is reduced from the transverse momentum [22]. As already shown in Ref. [28], such helical molecules can be adiabatically pumped by slowly rotating the external electric field and hence modulating the on-site energy periodically in time, which shares the same topological origin as the integer quantum Hall effect [6,7]. The main ingredient of the present work is to investigate consequences of the long-range hopping t_j in this topological Thouless pump. We would like to further mention that apart from the protein- and DNA-inspired models, Hamiltonians like Eq. (1) can also describe other helical lattices in a broader context, e.g., for ultracold atoms trapped on helical space curves [58]. In fact, helices constitute a quite intriguing model. Rich physical behaviors arising from the helical geometry have already been extensively studied in the past for quantum [58–62] and classical [63–67] setups, although in the nontopological aspect.

Our computational scheme is straightforward. Considering $\varphi(t)$ to be a time-independent variable parameter φ, we diagonalize the time-independent Hamiltonian (1) with finite molecular lengths and open boundary conditions to obtain the single-particle eigenenergies E_l and eigenstates ψ_l. From this spectrum, the end states and the spatial distribution of electron density $P_{ln} = |\psi_{ln}|^2$ can be identified (ψ_{ln} is the amplitude of the lth eigenstate ψ_l at site n). For helical molecules with infinite length, the longitudinal momentum k defined within the first Brillouin zone (BZ) is a good quantum number. After the Fourier transform, diagonalizing the Hamiltonian (1) ($N \to \infty$) in the momentum space yields the Bloch state $u_i(k, \varphi)$ corresponding to the ith energy band $E_i(k, \varphi)$. In this case, the bulk band topology is characterized by the first Chern number [22,25]

$$C_i = -\frac{1}{\pi} \int_{\mathrm{BZ}} dk \int_0^{2\pi} d\varphi \, \mathrm{Im}\left\langle \frac{\partial u_i(k,\varphi)}{\partial k} \middle| \frac{\partial u_i(k,\varphi)}{\partial \varphi} \right\rangle, \qquad (3)$$

which is a $\mathbb{Z}$ topological invariant.

In order to calculate the current pumped adiabatically by the slowly rotating electric field, the explicit time dependences of the phase $\varphi(t)$ and thus the Hamiltonian (1) need to be considered. This does not mean that $\mathcal{H}(t)$ is a truly driven system, but with its eigenenergy $E_l(t)$, eigenstate $\psi_l(t)$, and the electron density $P_{ln}(t)$ always taken to be the instantaneous ones for the parameter configuration at time t. To allow the current to flow through the system, we attach two electrodes to the helical molecule (see Fig. 1): the left (L) lead is coupled to the first site, and the right (R) lead is coupled to the last site. The additional Hamiltonian terms are

$$\mathcal{H}_0 = \sum_{\mathbf{k},\alpha} \varepsilon_{\mathbf{k}} c_{\mathbf{k}\alpha}^\dagger c_{\mathbf{k}\alpha} + \sum_{\mathbf{k},\alpha} t_0(c_{\mathbf{k}\alpha}^\dagger c_{n_\alpha} + \mathrm{H.c.}), \qquad (4)$$

where $\alpha = L/R$, $n_L = 1$, $n_R = N$, $c_{\mathbf{k}\alpha}^\dagger$ ($c_{\mathbf{k}\alpha}$) creates (annihilates) an electron with momentum $\mathbf{k}$ and energy $\varepsilon_{\mathbf{k}}$ in the α lead, and t_0 is the tunneling amplitude between the leads and the end sites of the molecule. It is convenient to introduce the quantity $\Gamma = 2\pi \rho t_0^2$, with ρ being the density of lead states, to represent the lead-molecule coupling strength. Note that there is no bias voltage between the two leads; that is, they are held at the same chemical potential, having the same Fermi energy E_F. Under the adiabatic approximation, the system is time independent at every instant. We can calculate the instantaneous current for the parameters at every t and then integrate it over one pump cycle to obtain the pumped current. Specifically, the instantaneous current $I(t)$ flowing from the L lead to the molecule is given by the time derivative of the electron number $M = \sum_{\mathbf{k}} c_{\mathbf{k}L}^\dagger c_{\mathbf{k}L}$ of the L lead,

$$I(t) = -e\frac{d}{dt}\langle M \rangle = -\frac{e}{i\hbar}\langle[M, \mathcal{H}(t) + \mathcal{H}_0]\rangle. \qquad (5)$$

It is convenient to rewrite $\mathcal{H}(t)$ and $\mathcal{H}_0$ in the basis of instantaneous eigenstates,

$$\mathcal{H}(t) = \sum_{l=1}^N E_l(t) d_l^\dagger d_l, \qquad (6)$$

$$\mathcal{H}_0(t) = \sum_{\mathbf{k},\alpha} \varepsilon_{\mathbf{k}} c_{\mathbf{k}\alpha}^\dagger c_{\mathbf{k}\alpha}$$
$$+ \sum_{\mathbf{k},\alpha} \sum_{l=1}^N t_0 \psi_{ln_\alpha}(t)(c_{\mathbf{k}\alpha}^\dagger d_l + \mathrm{H.c.}), \qquad (7)$$

with $d_l = \sum_{n=1}^N \psi_{ln}(t)c_n$. Substituting Eqs. (6) and (7) into Eq. (5), one obtains $I(t) = \sum_{l=1}^N I_l(t)$ and

$$I_l(t) = \frac{ie}{\hbar}\sum_{\mathbf{k}} t_0 \psi_{l1}(t)(\langle c_{\mathbf{k}L}^\dagger d_l \rangle - \langle d_l^\dagger c_{\mathbf{k}L} \rangle). \qquad (8)$$

Using the Keldysh nonequilibrium Green's function technique and the Dyson equations [68,69], the current through the lth eigenstate $I_l(t)$ reads

$$I_l(t) = \frac{ie\Gamma}{\hbar} P_{l1}(t) \int \frac{d\varepsilon}{2\pi}\left[G_l^<(\varepsilon, t) + 2if_{\mathrm{FD}}(\varepsilon)\mathrm{Im}G_l^r(\varepsilon, t)\right], \qquad (9)$$

where $f_{\mathrm{FD}}(\varepsilon)$ is the Fermi-Dirac distribution function and $G_l^{<,r}(\varepsilon, t)$ are the Fourier transforms of the lesser ($<$) and retarded (r) Green's functions of the lth eigenstate for system parameters at time t. While the integral of $G_l^<(\varepsilon, t)$ gives the

electron occupation $m_l(t)$ of the lth eigenstate,

$$\int \frac{d\varepsilon}{2\pi} G_l^<(\varepsilon, t) = i\langle d_l^\dagger d_l \rangle = im_l(t), \tag{10}$$

the second term of Eq. (9) can be calculated as

$$\int \frac{d\varepsilon}{2\pi} f_{FD}(\varepsilon) \text{Im} G_l^r(\varepsilon, t)$$

$$= \int \frac{d\varepsilon}{2\pi} \frac{-f_{FD}(\varepsilon) \widetilde{\Gamma}/2}{[\varepsilon - E_l(t)]^2 + \frac{\widetilde{\Gamma}^2}{4}}$$

$$\simeq -f_{FD}[E_l(t)] \int \frac{d\varepsilon}{2\pi} \frac{\widetilde{\Gamma}/2}{[\varepsilon - E_l(t)]^2 + \frac{\widetilde{\Gamma}^2}{4}}$$

$$= -\frac{1}{2} f_{FD}[E_l(t)]. \tag{11}$$

The second line of Eq. (11) assumes that $\widetilde{\Gamma} \equiv \Gamma(P_{l1} + P_{lN})$ is sufficiently small such that $f_{FD}(\varepsilon)$ is a slowly varying function near $E_l(t)$ and can be taken out of the integral. Substituting Eqs. (10) and (11) into Eq. (9) leads to

$$I_l(t) = \frac{e\Gamma}{\hbar} P_{l1}(t)\{f_{FD}[E_l(t)] - m_l(t)\}. \tag{12}$$

Here $m_l(t)$ evolves obeying the equation of motion,

$$\frac{dm(t)}{dt} = \frac{1}{i\hbar} \langle [d_l^\dagger d_l, \mathcal{H}(t) + \mathcal{H}_0] \rangle. \tag{13}$$

Following a procedure similar to that for calculating the current, it is readily found that

$$\frac{dm_l(t)}{dt} = \frac{\Gamma}{\hbar} [P_{l1}(t) + P_{lN}(t)]\{f_{FD}[E_l(t)] - m_l(t)\}. \tag{14}$$

Consequently, we can self-consistently solve Eq. (14) to determine the electron occupation $m_l(t)$ of the lth eigenstate and then obtain the current $I_l(t)$ by Eq. (12).

It is defined that the adiabatically pumped current is the average current over one pump cycle. Therefore, the integral,

$$I_l = f \int_0^{\frac{1}{f}} I_l(t) \, dt, \tag{15}$$

gives the pumped current through the lth eigenstate and the total pumped current $I = \sum_{l=1}^N I_l$.

III. RESULTS AND DISCUSSION

In the numerical results presented below, we fix the nearest-neighbor hopping $t_1 = 0.1$ eV as the energy unit, $V_g = 1.5t_1$, the twist angle $\phi_0 = 2\pi/5$, and the molecular length $N = 100$, unless stated otherwise. To calculate the pumped current, we take the lead-molecule coupling $\Gamma = 10^{-6}t_1$ and the rotational frequency $f = 10^5$Hz, such that the adiabatic condition, $hf \ll \Gamma, t_1$ (h is the Planck constant), always holds. The temperature T is set to be $k_BT = 0$ (k_B the Boltzmann constant), unless stated otherwise.

A. Bulk topology and end states

Before investigating the consequence of long-range hopping on the adiabatic pumping, it is helpful to examine first its effect on the bulk topology and end states by considering the orientation $\varphi(t)$ of electric field as a time-independent but variable parameter φ. Figure 2 presents the energy spectra of single-helical organic molecules as functions of the phase φ [Figs. 2(a)–2(d)] and the momentum k [Figs. 2(e)–2(h)] with finite length under open boundary conditions and infinite length, respectively, for different long-range decay exponents μ. In either case, the molecule possesses five energy bands (bands 1–5, bottom to top) separated by four gaps [gaps I–IV, bottom to top; see, e.g., Fig. 2(a)] since its unit cell contains five sites due to $\phi_0 = 2\pi/5$. These energy bands are asymmetric above and below zero energy because the presence of the long-range hoppings and/or the external electric field breaks the electron-hole symmetry of the system. Interestingly, there is a pair of end states in each energy gap. As the phase φ varies, these state pairs, denoted by colored lines in Figs. 2(a)–2(d), traverse the gaps and intersect at some values of φ. For odd numbers of intersection points [see gaps I and IV in Figs. 2(a)–2(d) and gap III in Fig. 2(c)], the electronic states at $\varphi = 0$ and 2π on the same colored line are different, signaling an evolutionary cycle of 4π just like a Möbius strip. When the number of intersection points is even [see gap II in Figs. 2(a)–2(d) and gap III in Figs. 2(a) and 2(d)], the evolutionary period is 2π.

The most striking feature lies in the evolution of energy spectra with the variation of the long-range hoppings. It is shown in Fig. 2 that upon decreasing the decay exponent μ (i.e., enhancing the long-range hoppings), the system undergoes a topological phase transition at a critical decay exponent $\mu_c \simeq 1.145$. For $\mu > \mu_c$ [Figs. 2(a), 2(d), 2(e), and 2(h)], gap III exists, and the two midgap end states intersect twice as a function of φ with a period of 2π. Gap III closes at $\mu = \mu_c$ [Figs. 2(b) and 2(f)] and reopens for $\mu < \mu_c$ [Figs. 2(c) and 2(g)]. In the latter case, the two midgap end states intersect three times as a function of φ with a period of 4π. Therefore, the transition at the critical decay exponent separates two topologically distinct phases of the system. Note that gaps I, II, and IV and the φ evolutions of the end states in these gaps do not change qualitatively in the whole range of μ.

This topological phase transition driven by the long-range hoppings is also manifested in the bulk topology characterized by the Chern numbers. As the decay exponent μ increases past the critical value μ_c, the Chern number C_3 of band 3 jumps from 1 to −4, while the Chern number C_4 of band 4 jumps backwards [Fig. 3(a)]. On the other hand, the Chern numbers of bands 1, 2, and 5 are always 1 for arbitrary μ [inset of Fig. 3(a)], indicating that no phase transition occurs in these energy bands. For systems with different twist angles ϕ_0, this topological phase transition is rather universal. Indeed, the phase transition always occurs in helical molecules with more than two sites in the unit cell ($2\pi/\phi_0 \geqslant 3$), although it is absent when the unit cell contains only two sites ($2\pi/\phi_0 = 2$). We plot in Fig. 3(b) the critical decay exponent μ_c as a function of the site number $2\pi/\phi_0$ in the unit cell, where μ_c overall increases with $2\pi/\phi_0$ but exhibits an even-odd oscillation.

To further elucidate the distinct topological nature of the two phases separated by the transition at $\mu = \mu_c$, we study the spatial distribution of electronic states marked by the two magenta lines pertinent to gap III [see Figs. 2(a)–2(d)]. Depending on the values of the phase φ, these states are
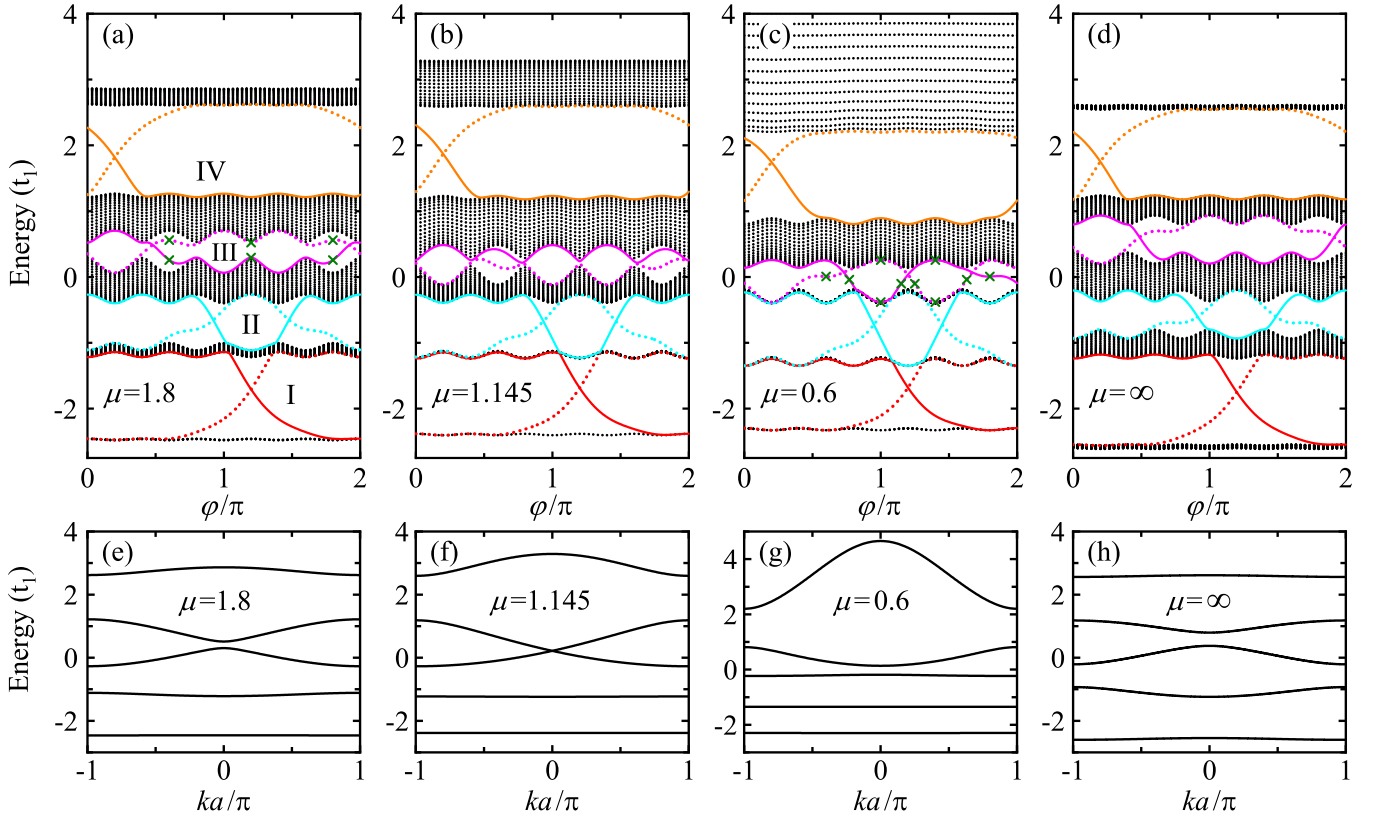
FIG. 2. (a)–(d) Energy spectra of single-helical organic molecules with finite length under open boundary conditions for different long-range decay exponents μ as a function of the phase φ. The colored lines indicate the evolutions of electronic states traversing energy gaps, and the green crosses mark the electronic states whose spatial distributions are shown in Fig. 4. (e)–(h) Energy bands of single-helical molecules with infinite length for different μ at fixed $\varphi = 0$. Here a in the abscissa label ka/π denotes the lattice constant. (d) and (h) are energies in the absence of long-range hoppings, shown for completeness.

localized at the left end (L) or right end (R) of the molecule, when the lines are within the energy gap. They can also be extended states (E) distributed in the whole system when the lines merge into band 3 or band 4. More specifically, in the topological phase of weak long-range hoppings ($\mu > \mu_c$), by varying φ from zero to 2π, the spatial distributions of the states along the solid and dotted magenta lines in Figs. 2(a) and 2(d) evolve following

$$\text{solid: } \text{E} \rightarrow \boxed{\text{R} \rightarrow \text{E} \rightarrow \text{L}} \rightarrow \text{E}, \tag{16}$$

$$\text{dotted: } \text{R} \rightarrow \text{E} \rightarrow \boxed{\text{L} \rightarrow \text{E} \rightarrow \text{R}}. \tag{17}$$

respectively. Here the evolutionary steps contributing to the charge pumping (see Sec. III B) are enclosed by boxes, and their typical spatial distributions are shown in Figs. 4(a)– 4(c). In the topological phase of strong long-range hoppings ($\mu < \mu_c$), the evolutions of these states are

$$\text{solid: } \text{E} \rightarrow \boxed{\text{L} \rightarrow \text{E} \rightarrow \text{R} \rightarrow \text{E} \rightarrow \text{L}}, \tag{18}$$

$$\text{dotted: } \text{L} \rightarrow \text{E} \rightarrow \boxed{\text{R} \rightarrow \text{E} \rightarrow \text{L} \rightarrow \text{E} \rightarrow \text{R}} \rightarrow \text{E}, \tag{19}$$

for the solid and dotted magenta lines in Fig. 2(c), respectively, and Figs. 4(d)–4(h) present the typical spatial

distributions of the contributing steps that are enclosed by boxes in Eqs. (18) and (19). Obviously, the spatial evolutions of the states in gap III are very different between the weak- and strong-hopping phases. This difference in the spatial distributions of end states as a function of φ will have important consequences in the charge pumping effect discussed subsequently. At the critical point $\mu = \mu_c$, although gap III is closed, the electronic states in the magenta lines can still be localized at the molecular ends (not shown here) for some values of φ at which the lines do not merge into the bands. One more notable feature is that in some variation ranges of the phase φ, the energy of a certain end state can be a nonmonotonic function of φ, and its slope can change sign; see, e.g., the dotted magenta line in Fig. 2(a) in the range of $0.4\pi < \varphi < 0.8\pi$. Hence, there is no one-to-one correspondence between the slopes of the midgap end states and the end they localize on in our system.

B. Topological charge pumping

We now turn to investigate the adiabatic charge pumping in single-helical organic molecules with long-range hoppings. The focus is on demonstrating how the topological phase transition driven by the long-range hoppings is manifested in the pumped current through the system. The general rule for electronic tunnelings between the molecule and the electrodes
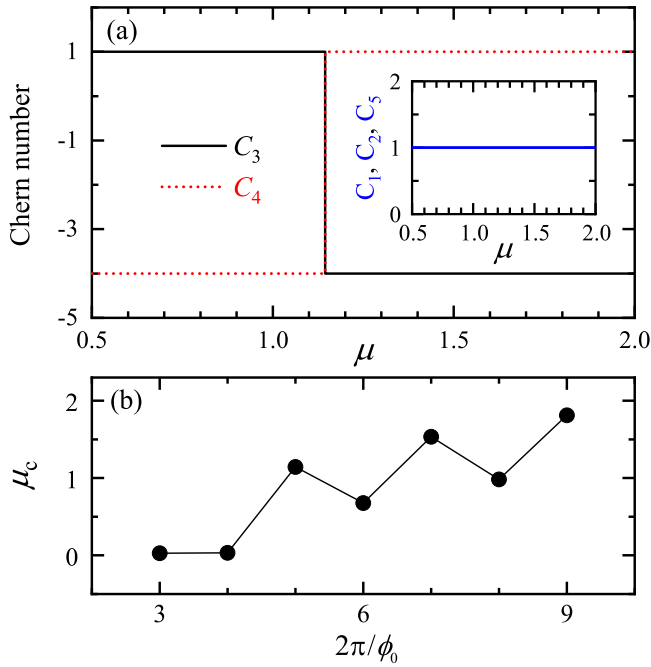
FIG. 3. (a) Chern numbers, C_1–C_5, for the five energy bands of the single-helical molecule as a function of the long-range decay exponent μ. C_3 and C_4 jump at the critical value, $\mu_c \simeq 1.145$, of the decay exponent, indicating the topological phase transition. (b) Dependence of the critical decay exponent μ_c on the twist angle ϕ_0. $2\pi/\phi_0$ gives the number of sites in each unit cell.
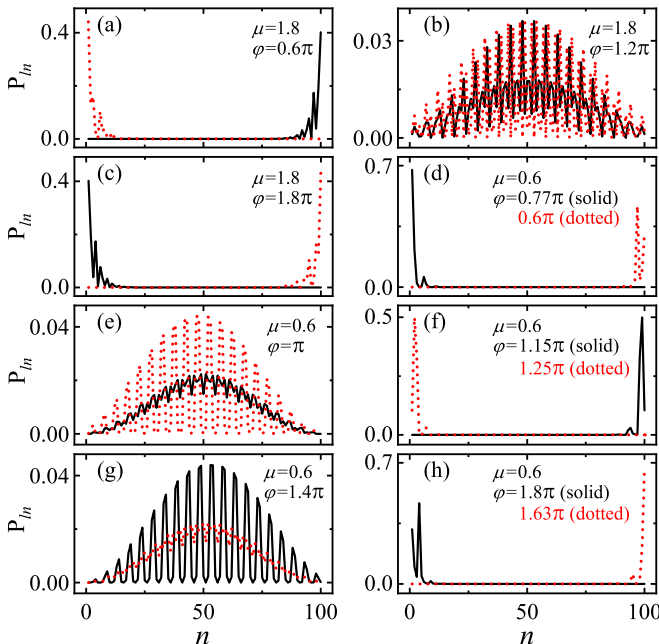

FIG. 4. Spatial distributions of electron density P_{ln} for the 16 electronic states marked by the 16 green crosses shown in Figs. 2(a) and 2(c), with solid (dotted) lines here corresponding to the solid (dotted) lines there. The specific phase values of these states are shown in each panel. More specifically, (a)–(c), with $\mu = 1.8$, display the typical spatial evolutions of the two end states in gap III in the weak-hopping topological phase, while (d)–(h), with $\mu = 0.6$, are in the strong-hopping topological phase.
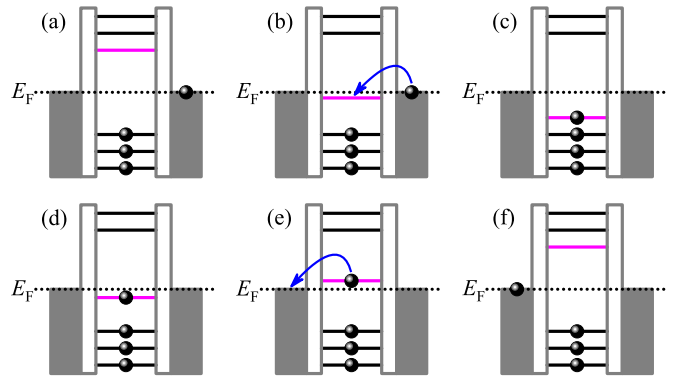

FIG. 5. Schematic diagrams of the charge pumping process in single-helical organic molecules coupled with two electrodes. (a)–(f) correspond to the phase $\varphi(t)$ evolving in time from zero to 2π. The magenta lines here represent the energy levels marked by the solid magenta line in Fig. 2(a), and the black balls symbolize electrons.

is as follows. At zero temperature, any molecular states with energy higher (lower) than the Fermi energy E_F must be empty (occupied). Therefore, when a molecular state moves downwards (upwards) across E_F, it changes from empty (occupied) to occupied (empty), and there must be an electron tunneling into (out of) the molecule. Taking the end state indicated by the solid magenta line in Fig. 2(a) as an example in the weak-hopping ($\mu > \mu_c$) phase, we illustrate in Fig. 5 the physical mechanism of electronic transport through topological end states driven by the slowly rotating electric field. Placing the Fermi energy E_F in the middle of gap III, we start with the initial state at the zero phase $\varphi(t) = 0$. This initial state in the solid magenta line is an extended state which lies above E_F and touches the bottom of band 4 [Figs. 2(a) and 5(a)]. Under adiabatic modulation of the pumping parameter $\varphi(t)$ by rotating the electric field, the state evolves with time. Specifically, as $\varphi(t)$ increases from zero to π, the state is dragged downwards from the bottom of band 4 to the top of band 3 [Figs. 5(a)–5(c)], and its spatial distribution evolves according to $E \to R \to E$ [Eq. (16)]. During this process, the state is localized at the right end of the molecule while it moves downwards across the Fermi energy. An electron can then tunnel into the molecule from the right electrode [Fig. 5(b)]. Further adjusting $\varphi(t)$ from π to 2π pushes the state from the top of band 3 up to the bottom of band 4 [Figs. 5(c)–5(f)], and its spatial distribution changes as $E \to L \to E$ [Eq. (16)]. In particular, the electron is transferred to the left electrode because the state is now localized at the left end of the molecule while passing upwards through the Fermi energy [Fig. 5(e)]. Therefore, over each pump cycle, one electron is pumped from the right electrode to the left one across the molecule. The evolutionary steps contributing to this pumping process are $R \to E \to L$, as enclosed by the box in Eq. (16). For the state marked by the dotted magenta line in gap III [Fig. 2(a)], the contributing evolutionary steps are $L \to E \to R$ [see the box in Eq. (17)], which first transfer an electron from the molecule to the left electrode and then another electron from the right electrode to the molecule. The overall effect is also that one electron is pumped from the right electrode to the left one over each pump cycle. As a result, in
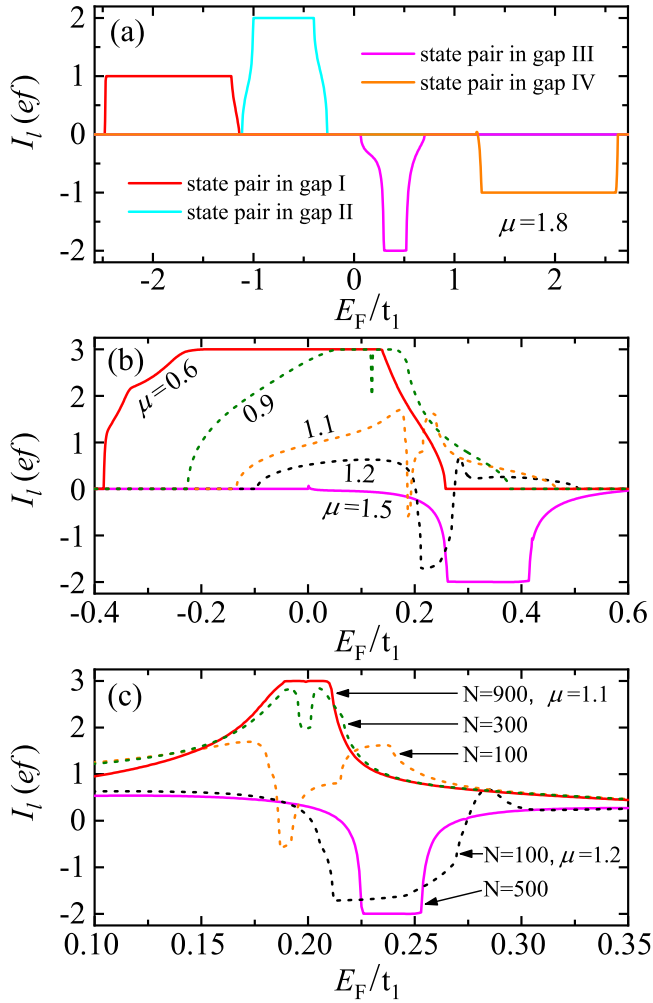
FIG. 6. (a) Pumped current I_l through end state pairs in gaps I–IV as a function of the Fermi energy E_F in the leads at the long-range decay exponent $\mu = 1.8$ greater than the critical value $\mu_c \simeq 1.145$. (b) Pumped current I_l through the state pair in gap III versus E_F for different μ. (c) Pumped current I_l through the state pair in gap III versus E_F for different molecular lengths N at two decay exponents μ very close to the critical value μ_c.
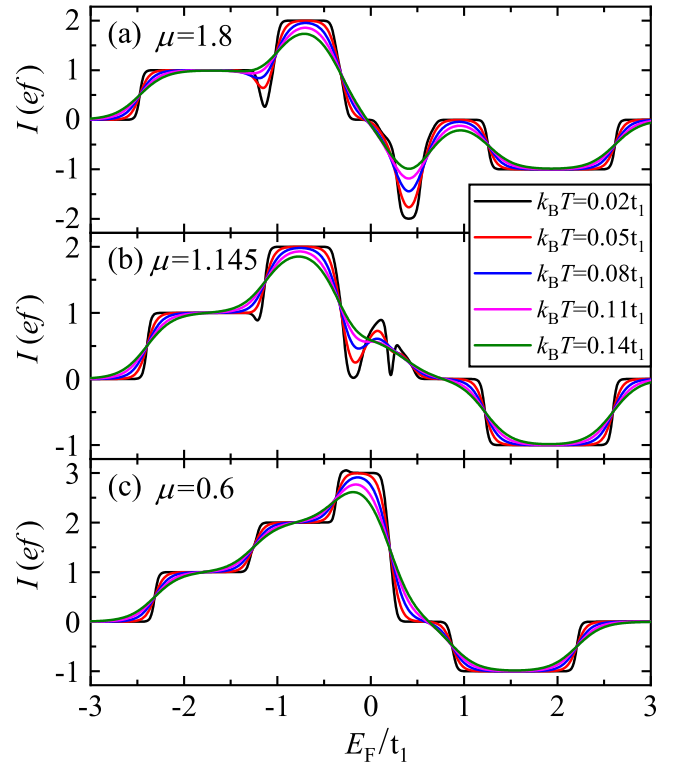

FIG. 7. Total pumped current I through all end states in the four band gaps as a function of the Fermi energy E_F at different temperatures T for different long-range decay exponents μ (a) in the $\mu > \mu_c$ phase, (b) at the critical point $\mu = \mu_c \simeq 1.145$, and (c) in the $\mu < \mu_c$ phase, respectively.

the weak-hopping ($\mu > \mu_c$) phase, the pumped current carried by the two end states in gap III, as a function of E_F, develops a plateau at $-2ef$ [see the magenta line in Fig. 6(a)], when E_F is in the gap, and thus, the system behaves as a Chern insulator. The minus here represents the current direction from the left to the right. Remarkably, the index theorem [70] relates the number of pumped electrons after one cycle and the sum of Chern invariants of occupied bands below gap III. The current plateau can then be written as $-2ef = \sum_{i=1}^{3} C_i ef$, establishing the bulk-boundary correspondence [22,70]. Note that $|C_1 + C_2 + C_3|$ also counts the number of intersections of the two end states in gap III as $\varphi(t)$ runs in $[0, 2\pi]$.

Similar analyses are equally applicable to the pumped current carried by the topological end states in other bulk gaps. Specifically, in the topological phase of weak long-range hoppings ($\mu > \mu_c$), when the Fermi energy sweeps through gaps I, II, and IV, the sum of Chern numbers of occupied bands is

$C_1 = 1$, $C_1 + C_2 = 2$, and $\sum_{i=1}^{4} C_i = -1$, respectively. These give rise to quantized current plateaus of ef, $2ef$, and $-ef$, as shown in Fig. 6(a). The heights of these current plateaus do not change quantitatively even in the strong-hopping ($\mu < \mu_c$) phase [see Fig. 7(c)] because the topological nature of the end state pairs in gaps I, II, and IV is robust against arbitrary amplitudes of the long-range hoppings.

However, the sum of Chern numbers of bands below gap III, $\sum_{i=1}^{3} C_i$, changes abruptly from -2 to 3 as μ reduces to the $\mu < \mu_c$ regime [Fig. 3(a)]. A current plateau of $3ef$ is thus expected when the Fermi energy sweeps through gap III [see the red line in Fig. 6(b)]. Just like the analyses in the $\mu > \mu_c$ case, this current plateau can also be understood by analyzing the specific pumping processes. In the topological phase of strong long-range hoppings ($\mu < \mu_c$), for the state along the solid magenta line in gap III [Fig. 2(c)], the contributing evolutionary steps [see the box in Eq. (18)] can first pump an electron from the left electrode to the right electrode and then another electron from the left electrode to the molecule. This is equivalent to transferring 1.5 (3) electrons from the left to the right electrode in one (two) cycle(s). The same is true for the contributing steps of the state marked by the dotted magenta line. Therefore, the end state pair in gap III totally pumps three electrons in one cycle, producing a current plateau at $3ef$ in the $\mu < \mu_c$ phase.

Figure 6(b) depicts the pumped current carried by the end state pair in gap III as a function of the Fermi energy E_F for

different decay exponents ranging from $\mu > \mu_c$ to $\mu < \mu_c$. It is shown that the current plateau features a continuous crossover from $-2ef$ to $3ef$, rather than a sudden jump typical for phase transitions, due to the finite-size effect [71,72]. For decay exponents μ close to the critical value μ_c and short molecular lengths N, the width of gap III can be comparable to the interval between adjacent energy levels in bulk bands, so that the gap is not well defined, and the current plateau is absent. This finite-size effect can be circumvented when energy levels in each band constitute continuums by increasing the molecular length. Indeed, as demonstrated in Fig. 6(c), for sufficiently long lengths, the pumped current carried by the end states in gap III always exhibits a well-formed plateau at either $-2ef$ (for $\mu > \mu_c$) or $3ef$ (for $\mu < \mu_c$), even though the decay exponents μ are very close to the critical value.

Since the adiabatic pumping effect is protected by the bulk topology of the helical molecules, it should generally be robust against perturbations such as disorder and many-body interaction [73]. Nevertheless, helical organic molecules could undergo a series of structural deformations, such as longitudinal stretching and squeezing, radial variations, and twisting and bending [35–39]. It is certainly worthwhile to further study how the revealed transport features, characteristic of the topological phase transition, are affected in all these cases, but for now we will not perform such a study in this paper. Instead, we would like to estimate the observability of these transport characteristics at finite temperatures. Figure 7 presents the temperature evolution of the total pumped current carried by all end states. Regardless of whether the system is in the weak-hopping ($\mu > \mu_c$) phase [Fig. 7(a)], in the strong-hopping ($\mu < \mu_c$) phase [Fig. 7(c)], or even at criticality [Fig. 7(b)], all relevant plateaus are well resolved in the total current when the Fermi energy sweeps consecutively through the four bulk gaps. As expected, these plateaus are smeared out with the temperature. The smearing mechanism is as follows. At finite temperatures, molecular states with energy higher (lower) than E_F still have a finite probability of being occupied (empty). Consequently, when a molecular state moves downwards (upwards) across E_F, there is a finite probability that an electron can tunnel out of (into) the molecule. These tunneling processes, opposite to those occurring at zero temperature [e.g., Figs. 5(b) and 5(e)], cancel the charge pumping, thus effectively smearing the current plateaus. Since the plateau widths are roughly given by the corresponding gap widths, the wider the gap is, the higher the temperature at which the current plateau can persist is. We find that the current plateau at $-2ef$, characteristic of the weak-hopping ($\mu > \mu_c$) phase, remains visible at the temperature $k_BT = 0.02t_1$ [Fig. 7(a)], while in the strong-hopping ($\mu < \mu_c$) phase, the characteristic plateau of $3ef$ can persist up to the temperature $k_BT = 0.05t_1$ [Fig. 7(c)]. These give out relatively high temperatures $T \simeq 23$ K and 58 K if

one takes the nearest-neighbor hopping $t_1 = 0.1$eV according to the first-principles calculations [31,74–76]. Although the exact temperature evolution of the pumped current plateaus depends on the specific model parameters used in this paper, there will be no qualitative changes when other values of the model parameters are used [28]. Therefore, we expect that the transport signature of the topological phase transition can be observed at finite temperatures in realistic DNA and protein molecules. Note that due to the downward shift of gap III when decreasing μ, the current plateaus of $-2ef$ and $3ef$ occur at different E_F. To experimentally achieve a switching between the two characteristic plateaus by tuning μ, one needs to either shift E_F accordingly or counteract the band shift somehow (e.g., by simultaneously tuning E the electric field strength).

IV. CONCLUSION

We have studied the topological adiabatic pumping of electrons in single-helical organic molecules with long-range hoppings. We showed that the strong and weak long-range hopping regimes represent two topologically distinct phases of the system, which are separated by a topological phase transition with characteristic features manifested in the molecular band structure and in the pumped current. In particular, the strong- and weak-hopping phases support the transport of pumped electrons in opposite directions, resulting in the quantized plateau in the pumped current as a function of the Fermi energy exhibiting different signs and amplitudes between the two phases. Due to the finite lengths of the molecules, we observe a smooth crossover, rather than a sharp reversal, of the current plateau near the topological criticality, which is experimentally accessible in realistic helical molecules. The study of topological physics in helical organic and bioorganic molecular systems is still in its infancy. We hope the present paper will attract more research interest in this direction. Besides being fundamentally interesting in their own right, such studies could also provide novel designing principles for molecular electronic devices by exploiting their topological phases.

[1] K. v. Klitzing, G. Dorda, and M. Pepper, Phys. Rev. Lett. **45**, 494 (1980).

[2] D. C. Tsui, H. L. Stormer, and A. C. Gossard, Phys. Rev. Lett. **48**, 1559 (1982).

[3] F. D. M. Haldane, arXiv:1612.00076.

[4] F. D. M. Haldane, Phys. Lett. A **93**, 464 (1983).

[5] F. D. M. Haldane, Phys. Rev. Lett. **50**, 1153 (1983).

[6] D. J. Thouless, M. Kohmoto, M. P. Nightingale, and M. den Nijs, Phys. Rev. Lett. **49**, 405 (1982).

[7] M. Kohmoto, Ann. Phys. (NY) **160**, 343 (1985).

[8] C. L. Kane and E. J. Mele, Phys. Rev. Lett. **95**, 226801 (2005); **95**, 146802 (2005).

[9] B. A. Bernevig, T. L. Hughes, and S.-C. Zhang, Science **314**, 1757 (2006).

[10] B. A. Bernevig and S.-C. Zhang, Phys. Rev. Lett. **96**, 106802 (2006).

[11] M. König, S. Wiedmann, C. Brüne, A. Roth, H. Buhmann, L. W. Molenkamp, X.-L. Qi, and S.-C. Zhang, Science **318**, 766 (2007).

[12] J. E. Moore, Nat. Phys. **5**, 378 (2009); Nature (London) **464**, 194 (2010).

[13] M. Z. Hasan and C. L. Kane, Rev. Mod. Phys. **82**, 3045 (2010).

[14] X.-L. Qi and S.-C. Zhang, Rev. Mod. Phys. **83**, 1057 (2011).

[15] X.-L. Qi, T. L. Hughes, S. Raghu, and S.-C. Zhang, Phys. Rev. Lett. **102**, 187001 (2009).

[16] S. B. Chung and S.-C. Zhang, Phys. Rev. Lett. **103**, 235301 (2009).

[17] S. Murakawa, Y. Tamura, Y. Wada, M. Wasai, M. Saitoh, Y. Aoki, R. Nomura, Y. Okuda, Y. Nagato, M. Yamamoto, S. Higashitani, and K. Nagai, Phys. Rev. Lett. **103**, 155301 (2009).

[18] A. P. Schnyder and S. Ryu, Phys. Rev. B **84**, 060504(R) (2011).

[19] Z. Wang, Y. Sun, X.-Q. Chen, C. Franchini, G. Xu, H. Weng, X. Dai, and Z. Fang, Phys. Rev. B **85**, 195320 (2012).

[20] X. Wan, A. M. Turner, A. Vishwanath, and S. Y. Savrasov, Phys. Rev. B **83**, 205101 (2011).

[21] N. R. Cooper, J. Dalibard, and I. B. Spielman, Rev. Mod. Phys. **91**, 015005 (2019).

[22] T. Ozawa, H. M. Price, A. Amo, N. Goldman, M. Hafezi, L. Lu, M. C. Rechtsman, D. Schuster, J. Simon, O. Zilberberg, and I. Carusotto, Rev. Mod. Phys. **91**, 015006 (2019).

[23] C. A. Downing, T. J. Sturges, G. Weick, M. Stobińska, and L. Martín-Moreno, Phys. Rev. Lett. **123**, 217401 (2019).

[24] S. D. Huber, Nat. Phys. **12**, 621 (2016).

[25] D. J. Thouless, Phys. Rev. B **27**, 6083 (1983).

[26] S. Nakajima, T. Tomita, S. Taie, T. Ichinose, H. Ozawa, L. Wang, M. Troyer, and Y. Takahashi, Nat. Phys. **12**, 296 (2016).

[27] M. Lohse, C. Schweizer, O. Zilberberg, M. Aidelsburger, and I. Bloch, Nat. Phys. **12**, 350 (2016).

[28] A.-M. Guo and Q.-F. Sun, Phys. Rev. B **95**, 155411 (2017).

[29] H.-Z. Tang, Q.-F. Sun, J.-J. Liu, and Y.-T. Zhang, Phys. Rev. B **99**, 235427 (2019).

[30] A. V. Malyshev, Phys. Rev. Lett. **98**, 096801 (2007).

[31] R. G. Endres, D. L. Cox, and R. R. P. Singh, Rev. Mod. Phys. **76**, 195 (2004).

[32] P. Meredith, C. J. Bettinger, M. Irimia-Vladu, A. B. Mostert, and P. E. Schwenn, Rep. Prog. Phys. **76**, 034501 (2013).

[33] E. L. Albuquerque, U. L. Fulco, V. N. Freire, E. W. S. Caetano, M. L. Lyra, and F. A. B. F. de Moura, Phys. Rep. **535**, 139 (2014).

[34] C. D. Bostick, S. Mukhopadhyay, I. Pecht, M. Sheves, D. Cahen, and D. Lederman, Rep. Prog. Phys. **81**, 026601 (2018).

[35] J. Gore, Z. Bryant, M. Nöllmann, M. U. Le, N. R. Cozzarelli, and C. Bustamante, Nature (London) **442**, 836 (2006).

[36] T. Lionnet, S. Joubaud, R. Lavery, D. Bensimon, and V. Croquette, Phys. Rev. Lett. **96**, 178102 (2006).

[37] P. Gross, N. Laurens, L. B. Oddershede, U. Bockelmann, E. J. G. Peterman, and G. J. L. Wuite, Nat. Phys. **7**, 731 (2011).

[38] B. Đuričković, A. Goriely, and J. H. Maddocks, Phys. Rev. Lett. **111**, 108103 (2013).

[39] A. Löf, P. U. Walker, S. M. Sedlak, S. Gruber, T. Obser, M. A. Brehm, M. Benoit, and J. Lipfert, Proc. Natl. Acad. Sci. USA **116**, 18798 (2019).

[40] A.-M. Guo and Q.-F. Sun, Proc. Natl. Acad. Sci. USA **111**, 11658 (2014).

[41] D. Mishra, T. Z. Markus, R. Naaman, M. Kettner, B. Göhler, H. Zacharias, N. Friedman, M. Sheves, and C. Fontanesi, Proc. Natl. Acad. Sci. USA **110**, 14872 (2013).

[42] A.-M. Guo and Q.-F. Sun, Phys. Rev. Lett. **108**, 218102 (2012).

[43] B. Göhler, V. Hamelbeck, T. Z. Markus, M. Kettner, G. F. Hanne, Z. Vager, R. Naaman, and H. Zacharias, Science **331**, 894 (2011).

[44] J. Stockhofe and P. Schmelcher, Phys. Rev. A **92**, 023605 (2015).

[45] S. Longhi, Europhys. Lett. **116**, 30005 (2016).

[46] C. H. Kim, H. S. Kim, H. Jeong, H. Jin, and J. Yu, Phys. Rev. Lett. **108**, 106401 (2012).

[47] B. Pérez-González, M. Bello, Á. Gómez-León, and G. Platero, Phys. Rev. B **99**, 035146 (2019).

[48] Y. Ke, X. Qin, F. Mei, H. Zhong, Y. S. Kivshar, and C. Lee, Laser Photonics Rev. **10**, 995 (2016).

[49] Y. Ke, X. Qin, Y. S. Kivshar, and C. Lee, Phys. Rev. A **95**, 063630 (2017).

[50] Z. Xu, Y. Zhang, and S. Chen, Phys. Rev. A **96**, 013606 (2017).

[51] C.-T. Shih, S. Roche, and R. A. Römer, Phys. Rev. Lett. **100**, 018105 (2008).

[52] G. Cuniberti, E. Maciá, A. Rodríguez, and R. A. Römer, in *Charge Migration in DNA: Perspectives from Physics, Chemistry and Biology*, edited by T. Chakraborty (Springer, Berlin, 2007).

[53] Z. G. Yu and X. Song, Phys. Rev. Lett. **86**, 6018 (2001).

[54] A.-M. Guo and Q.-F. Sun, Phys. Rev. B **86**, 035424 (2012).

[55] T.-R. Pan, A.-M. Guo, and Q.-F. Sun, Phys. Rev. B **92**, 115418 (2015).

[56] P. G. Harper, Proc. Phys. Soc. A **68**, 874 (1955).

[57] D. R. Hofstadter, Phys. Rev. B **14**, 2239 (1976).

[58] J. Stockhofe and P. Schmelcher, Phys. Rev. A **91**, 023606 (2015).

[59] J. K. Pedersen, D. V. Fedorov, A. S. Jensen, and N. T. Zinner, J. Phys. B **49**, 024002 (2016).

[60] O. V. Kibis, S. V. Malevannyy, L. Huggett, D. G. W. Parfitt, and M. E. Portnoi, Electromagnetics **25**, 425 (2005).

[61] E. L. Ivchenko and B. Spivak, Phys. Rev. B **66**, 155404 (2002).

[62] C. A. Downing, M. G. Robinson, and M. E. Portnoi, Phys. Rev. B **94**, 155306 (2016).

[63] J. Plettenberg, J. Stockhofe, A. V. Zampetaki, and P. Schmelcher, Phys. Rev. E **95**, 012213 (2017).

[64] A. V. Zampetaki, J. Stockhofe, and P. Schmelcher, Phys. Rev. A **91**, 023409 (2015).

[65] A. V. Zampetaki, J. Stockhofe, and P. Schmelcher, Phys. Rev. E **92**, 042905 (2015).

[66] A. V. Zampetaki, J. Stockhofe, and P. Schmelcher, Phys. Rev. E **95**, 022205 (2017).

[67] A. V. Zampetaki, J. Stockhofe, and P. Schmelcher, Phys. Rev. E **97**, 042503 (2018).

[68] Y. Meir and N. S. Wingreen, Phys. Rev. Lett. **68**, 2512 (1992).

[69] H. Haug and A.-P. Jauho, *Quantum Kinetics in Transport and Optics of Semiconductors*, 2nd ed. (Springer, Berlin, 2008).

[70] C.-K. Chiu, J. C. Y. Teo, A. P. Schnyder, and S. Ryu, Rev. Mod. Phys. **88**, 035005 (2016).

[71] *Finite Size Scaling and Numerical Simulation of Statistical Systems*, edited by V. Privman (World Scientific, Singapore, 1990).

[72] D. J. Amit and V. Martin-Mayor, *Field Theory, the Renormalization Group, and Critical Phenomena*, 3rd ed. (World Scientific, Singapore, 2005).

[73] Q. Niu and D. J. Thouless, J. Phys. A **17**, 2453 (1984).

[74] Y. J. Yan and H. Zhang, J. Theor. Comput. Chem. **1**, 225 (2002).

[75] K. Senthilkumar, F. C. Grozema, C. F. Guerra, F. M. Bickelhaupt, F. D. Lewis, Y. A. Berlin, M. A. Ratner, and L. D. A. Siebbeles, J. Am. Chem. Soc. **127**, 14894 (2005).

[76] L. G. D. Hawke, G. Kalosakas, and C. Simserides, Eur. Phys. J. E **32**, 291 (2010).